Biofilm 5 (2023) 100113

Contents lists available at ScienceDirect

Biofilm

journal homepage: www.sciencedirect.com/journal/biofilm

Impact of mucus and biofilm on antimicrobial photodynamic therapy: Evaluation using Ruthenium(II) complexes

Raphaëlle Youf [a], Rosy Ghanem [a,b], Adeel Nasir [a], Gilles Lemercier [c], Tristan Montier [a,b,d], Tony Le Gall [a,*]

[a] Inserm, Univ Brest, EFS, UMR 1078, GGB, F-29200, Brest, France
[b] CHU de Brest, Service de Génétique Médicale et de Biologie de la Reproduction, 29200, Brest, France
[c] Université de Reims Champagne-Ardenne, UMR CNRS 7312, BP 1039, CEDEX 2, 51687, Reims, France
[d] CHU de Brest, Centre de Référence des Maladies Rares Maladies Neuromusculaires, 29200, Brest, France

ARTICLE INFO

Keywords:
Antimicrobial photodynamic therapy
Biofilm
Mucus
Photodynamic inactivation
Photosensitizer
Pulmonary infection

ABSTRACT

The biofilm lifestyle of bacterial pathogens is a hallmark of chronic lung infections such as in cystic fibrosis (CF) patients. Bacterial adaptation to the complex conditions in CF-affected lungs and repeated antibiotherapies lead to increasingly tolerant and hard-to-treat biofilms. In the context of growing antimicrobial resistance and restricted therapeutic options, antimicrobial photodynamic therapy (aPDT) shows great promise as an alternative to conventional antimicrobial modalities. Typically, aPDT consists in irradiating a non-toxic photosensitizer (PS) to generate reactive oxygen species (ROS), which kill pathogens in the surrounding environment. In a previous study, we reported that some ruthenium (II) complexes ([Ru(II)]) can mediate potent photodynamic inactivation (PDI) against planktonic cultures of *Pseudomonas aeruginosa* and *Staphylococcus aureus* clinical isolates. In the present work, [Ru(II)] were further assayed to evaluate their ability to photo-inactivate such bacteria under more complex experimental conditions better recapitulating the microenvironment in lung infected airways. Bacterial PDI was tentatively correlated with the properties of [Ru(II)] in biofilms, in mucus, and following diffusion across the latter. Altogether, the results obtained demonstrate the negative impacting role of mucus and biofilm components on [Ru(II)]-mediated PDT, following different possible mechanisms of action. Technical limitations were also identified that may be overcome, making this report a pilot for other similar studies. In conclusion, [Ru(II)] may be subjected to specific chemical engineering and/or drug formulation to adapt their properties to the harsh micro-environmental conditions of the infected respiratory tract.

1. Introduction

The lung micro-environment is characterized by various physiological parameters that may impact in different ways on antimicrobial treatments, especially in lower respiratory tract infections that are today the leading infectious cause of death worldwide [1]. Among the obstacles opposing the action of antimicrobials, biofilms can strongly limit the exposure of bacteria to the drugs delivered, thanks to the production of an adhesive and protective matrix composed of extracellular polymeric substances (EPS) [2,3]. The situation is even more complicated in diseases such as cystic fibrosis (CF) that is characterized by a dehydrated mucus acting as a supplementary barrier at the surface of the respiratory epithelium [4]. Generally speaking, it is essential to evaluate the possible effect(s) of the parameters defining the target environment to expect a therapeutic option to be translatable to clinical practice. Within this frame of reference, CF lung infection can be considered as a challenging model disease to develop therapeutic strategies, which may then be applied to other pulmonary infections.

CF is a genetic disorder with clinical manifestations taking place in many organs, with the most severe damages affecting the digestive and

Abbreviations: aPDT, antimicrobial photodynamic therapy; ASM, artificial sputum medium; CFU, colony forming unit; EPS, extracellular polymeric substances; OD, optical density; PDI, photodynamic inactivation; PS, photosensitizer; RFU, relative fluorescence unit; RT, room temperature; [Ru(II)], ruthenium(II) complexes; $^1O_2$, singlet oxygen.

* Corresponding author. Inserm, UMR 1078, Génétique, Génomique fonctionnelle et Biotechnologies, GTCA Team, Faculté de Médecine (UBO), 22 avenue Camille Desmoulins, 29238, Brest, France.
E-mail address: tony.legall@univ-brest.fr (T. Le Gall).

https://doi.org/10.1016/j.bioflm.2023.100113
Received 30 January 2023; Received in revised form 17 March 2023; Accepted 19 March 2023
Available online 24 March 2023
2590-2075/© 2023 The Authors. Published by Elsevier B.V. This is an open access article under the CC BY-NC-ND license (http://creativecommons.org/licenses/by-nc-nd/4.0/).

respiratory systems [5,6]. Ineffective mucociliary clearance promotes the accumulation of sticky and thick secretions in CF lungs that constitute a nutrient-enriched environment for opportunistic pathogens [7]. In addition, the alteration of physiological parameters (including local pH, salinity, and oxygenation) defines a specific pulmonary microenvironment that compromises the effectiveness of current antibiotherapeutic treatments [8,9]. Bacterial species such as *Staphylococcus aureus* and *Pseudomonas aeruginosa* are very well-adapted to the CF lung environment due to their genetic and phenotypic plasticity [10,11]. Their ability to form biofilms require the use of antibiotic doses 10 to 1000 times higher than against planktonic forms [12,13]. The development of bacterial biofilms inside the dehydrated CF mucus form an overall hard-to-cross physiological barrier for diverse therapeutic agents acting as antimicrobial, anti-inflammatory or gene drug [14–17].

In the context of increasing antimicrobial resistance, restricted remaining therapeutic options, and (re)emerging respiratory pandemics [18], antimicrobial photodynamic therapy (aPDT) holds great promise as a rescuing alternative modality [19,20]. This therapeutic approach is based on the illumination of a photosensitive molecule (called photosensitizer, PS) with light at a specific wavelength leading to the production of reactive oxygen species (ROS, including highly cytotoxic singlet oxygen $^1O_2$). The latter can inactivate a wide range of pathogens, independently of their drug-resistance profiles, and their multi-targeted action reduce the possibility for pathogens to develop resistance mechanisms [21,22]. Synthetic PS can exhibit better properties (especially as regard solubility and safety) than natural PS [23,24]. Among these, metal complexes such as ruthenium (II) complexes (hereafter abbreviated [Ru(II)]) constitute promising therapeutic candidates [25–29]. Previously, we examined the relevance of [Ru(II)]-based PDT as an antimicrobial strategy against CF bacterial isolates belonging to *S. aureus* and *P. aeruginosa* species [30]. A structure-activity study pointed out that different chemical parameters determined (i) the photophysical and physicochemical properties and (ii) the ability to interact with bacteria. In particular, engraftment of [Ru(II)] with Phen-T-Fluorenyl ligand(s) improved the affinity with bacteria, but also altered solubility and $^1O_2$ quantum yield. In another study, we studied the impact of various experimental parameters defining the CF lung microenvironment, including salinity, oxygenation and pH; mucus and biofilm were suggested to be main PDT suppressors, although more investigations were needed to better characterize the fate of [Ru(II)] in these matrices [31].

In the present study, a series of bioassays were conducted, to more precisely study the impact of mucus and biofilm on [Ru(II)]-based aPDT. For this purpose, we evaluated the ability of [Ru(II)] to exert PDI on bacteria in these media as well as following diffusion across a mucus layer; in every case, analytical methods were used to determine the concentration of PS as well as to detect the generation of singlet oxygen upon irradiation. Combining altogether the results obtained, we propose explanations and suggest improvements that may be useful for future studies using same or other PS (Fig. 1). Considering CF as a target application, the bacteria evaluated were *P. aeruginosa* and *S. aureus* and the mucus layer was a mimicking sputum medium (hereafter termed artificial sputum medium, ASM [31,32]).

2. Materials and methods

2.1. Materials

2.1.1. Photosensitizers

The photosensitizers used in this study were $[Ru(phen)_3]^{2+}(PF_6^-)_2$ (Ruthenium-tris(1, 10-phenanthroline) dihexafluorophosphate; molecular weight = 931.6 g/mol; Strem Chemicals, Inc) and $[Ru(bpy)_3]^{2+}(PF_6^-)_2$ (Ruthenium-tris(2,2′-bipyridyl) dihexafluorophosphate; molecular weight = 859.5 g/mol; Sigma Aldrich), hereafter noted **[Ru(II)] 1** and **[Ru(II)] 2**, respectively (Fig. 2). For each compound, 1 mg of powder was suspended in pure dimethyl sulfoxide (DMSO, Sigma Aldrich) to obtain a 5 mM stock solution. The latter was stored at room temperature (RT) in the dark and used no more than one week after.

2.1.2. Bacteria

The bacterial strains used were *S. aureus* RN4220 and *P. aeruginosa* Pa19660 (Schroeter, Migula ATCC® 19660™). For routine handling, they were subcultured on Luria Bertani (LB) agar plates incubated for 24 h at 37 °C then stored at 4 °C for two to three weeks. Liquid pre-cultures were prepared by inoculating a single bacterial colony in 5 mL of LB broth, followed by incubation at 37 °C under constant stirring for 16–18 h.

2.1.3. Specific media and other reagents

ASM consists of a mixture of porcine gastric mucin (Sigma Aldrich), salmon sperm single stranded DNA (Sigma Aldrich), diethylenetriaminepentaacetic acid (Sigma Aldrich), egg yolk emulsion (ThermoFischer Scientific), casaminoacids (MP Biomedicals), KCl (Sigma Aldrich) and NaCl (Sigma Aldrich). It was prepared as previously reported [31,32].

2.1.4. Devices

The microplate reader Mithras2 LB943 (Berthold) was used to perform optical density (OD) and fluorescence measurements, as previously described [31]. UV-visible and fluorescence spectra were done to check that absorbance and fluorescence signals were specific to [Ru

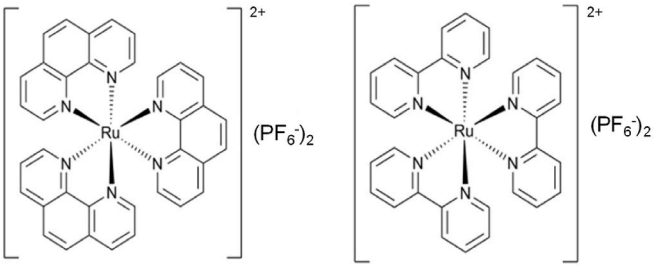

Fig. 2. Chemical structure of the photosensitizers used in this study. Phen, 1,10-phenanthroline; bpy, 2,2'-bipyridine; PF_6, hexafluorophosphate.

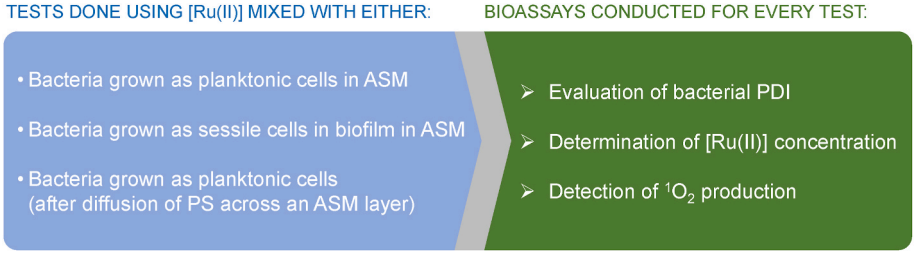

Fig. 1. Study design. Three tests were conducted that were each characterized using three types of bioassays.

(II)]. The light source used for PDI experiments was a custom-made device was described in a previous study [31]. It consisted of two panels each incorporating 225 14W pure blue (λ: 450–470 nm) light-emitting diodes (LEDs), providing a light power ~4 mW/cm^2 in the middle of the exposure area. Light treatments were performed, consisting of a first exposure to light for 15 min, then 15 min protected from light, and a second exposure to light for another 15 min. Light-treated and non-irradiated conditions are hereafter noted "ON" and "OFF", respectively.

2.2. Methods

2.2.1. PDI towards planktonic bacteria

[Ru(II)] solutions were prepared at 50 μM in water or in ASM before being added to 96-well plates (Sarstedt, Germany). The inocula of *S. aureus* RN4220 and *P. aeruginosa* PA19660 were then prepared as described above [23]. Briefly, 1 mL of each overnight culture was centrifuged at 2000 g for 10 min at 4 °C. The supernatants were discarded and the bacterial pellets were suspended in 0.9% NaCl. The OD at 600 nm of each solution was then readjusted to achieve inocula at 10^8 CFU/mL. Then, these solutions were diluted in 0.9% NaCl or in ASM to obtain 10^5 CFU/mL. The latter were distributed in a 96-well microplate (50 μL per well) containing 50 μL of [Ru(II)], thus achieving mixtures with $0.5.10^5$ CFU/mL and 25 μM [Ru(II)], either in 0.45% NaCl or in ASM. Each condition was replicated in 6 wells, three being exposed to light ("ON" conditions) and three kept in the dark ("OFF" conditions). After 10 min at RT, exposure to light was performed, as described above. Bacterial PDI was then evaluated using two methods. A first consisted in spotting 5 μL of each condition on a LB agar plate. Following an incubation for 18 h at 37 °C, the bacterial growth for each spot was checked, allowing to distinguish between no, intermediate or full PDI. The second method consisted in using 5 μL to inoculate 195 μL/well of LB medium in a 96 wellplate. The latter was placed inside the Mithras2 LB943 in order to read, every 10 min, the OD at 600 nm during 16 h at 30 °C. The kinetic growths obtained were then processed to determine the number of surviving cells in each condition, by comparing with bacteria that were not subjected to any treatment [30].

2.2.2. PDI towards bacteria in biofilm

Bacterial inocula of *S. aureus* and *P. aeruginosa* were prepared at 10^8 CFU/mL in saline as described in the previous section 2.2.1. Then, a dilution was performed to obtain inocula at 10^6 CFU/mL. The latter were distributed in a 96-well round bottom microplate (Costar) and mixed with [Ru(II)] or ciprofloxacin to achieve, by well, a final concentration of 50 μM and 32 μM, respectively, in 0.45% NaCl. After 10 min at RT, 50 μL of LB or ASM were added to each well then a membrane (Breathe-Easy® sealing membrane, Sigma-Aldrich) was used to cover the plate. After incubation at 37 °C under static condition for 20 h, the planktonic upper phase was carefully collected and transferred into a 96-well black-bottom wellplate (see next section). The isolated biofilms were then subjected to light treatment. Finally, the bacterial density was determined in each condition. For this purpose, each biofilm was suspended in 100 μL of 0.9% NaCl and thoroughly pipetted to dissociate it and obtain single bacteria. Serial dilutions were then performed and 5 μL of each dilution were deposited on LB agar plates. Following incubation at 37 °C for 18 h, single colonies were counted to estimate the bacterial density in each condition.

2.2.3. Determination of [Ru(II)] concentration

The concentration of [Ru(II)] in a given condition was estimated taking advantage of the peak absorption of these compounds at 455 nm or their fluorescence emission at 590 nm (following excitation at 460 nm). A range of known quantities of [Ru(II)] was assayed in the medium of interest so as to relate the signals obtained to a given amount of [Ru(II)]. (1) For quantifying in water or in ASM, [Ru(II)] solutions were prepared in either of these two media. After 10 min at RT, they were centrifuged at 2000 g for 5 min at 4 °C. The supernatant was collected and the pellet was suspended in water. Finally, OD at 455 nm was measured in both fractions. For each medium to assay, OD were subtracted to that measured with the corresponding medium-only i.e. without [Ru(II)] (see Figs. S1A–B for more details). (2) For quantifying [Ru(II)] in biofilms, the supernatant was carefully removed and biofilms were suspended before being transferred to a black 96-well plate. The [Ru(II)] fluorescence was measured in each condition and then normalized to that of control condition i.e. biofilms alone without [Ru(II)] (see Figs. S1C–D for more details).

2.2.4. Relative detection of $^1O_2$ production

The singlet oxygen sensor green (SOSG, Fisher Scientific) was used to detect the production of $^1O_2$ within ASM or biofilms. For this purpose, this reagent was mixed with the samples to assay at final concentration 10 μM, as recommended by the manufacturer. Before and after light treatment, the SOSG fluorescence was read with excitation at 504 ± 6 nm and emission at 525 ± 12 nm. Fluorescence signals were normalized to identify positive signals presumably reporting the production of $^1O_2$ due to the photo-activation of [Ru(II)] (Fig. S2).

2.2.5. Diffusion of [Ru(II)] across an ASM layer

Diffusion tests were carried out using 0.4 μm pore membrane inserts (Sarstedt) placed in a 24-well plate. For each condition to assay, four configurations were considered, as depicted in (Fig. 3).

After incubation for 4 h at RT, samples were collected from the donor and acceptor compartments in each configuration then used to measure absorbance at 455 nm. Subsequently, centrifugation was done at 2000 g for 5 min at 4 °C to isolate the supernatant from the pellet formed; the latter was suspended in water then absorbance was read in both fractions. The quantification of [Ru(II)] and $^1O_2$ was performed by using a standard range of [Ru(II)] in ASM and in water, as previously described. Finally, samples collected from the acceptor compartment were assayed with regard to PDI towards *S. aureus* and *P. aeruginosa*. After light treatment, the number of surviving cells in each condition was determined as detailed in section 2.2.1.

2.2.6. Interaction tests

To determine the potential interaction of [Ru(II)] with component(s) of interest, these were mixed then stored at RT for at least 5 min at RT. A centrifugation was then done at 2000 g for 5 min at 4 °C, to pellet the components studied and their possible aggregates with [Ru(II)]. Following collection of the supernatant, the pellet was suspended in the same volume as that of the supernatant. Finally, the fluorescence characteristic of [Ru(II)] was determined in each fraction. This allowed to estimate the distribution of [Ru(II)] in the supernatant and in the pellet, thus informing about the strength of the [Ru(II)] interaction with the component(s) evaluated.

2.2.7. Statistical analysis

The results presented correspond to the mean and standard deviation (mean ± SD) from the data obtained in independent experiments (N = 2) each including technical replicates (n = 3). Statistical analyses were performed by using the Student's t-test processed with Prism software version 7.00 (GraphPad). Statistically significant differences in pairwise comparisons were denoted as follows: ***, p-value ≤0.001; **, p-value ≤0.01; *, p-value ≤0.05. Non-significant differences were noted "ns".

3. Results

3.1. Impact of ASM

3.1.1. aPDT against planktonic bacteria in ASM

The two [Ru(II)] included in this study (Fig. 1) were first evaluated considering their ability to photo-inactivate planktonic forms of *S. aureus* or *P. aeruginosa* in ASM. For comparative purposes, the same

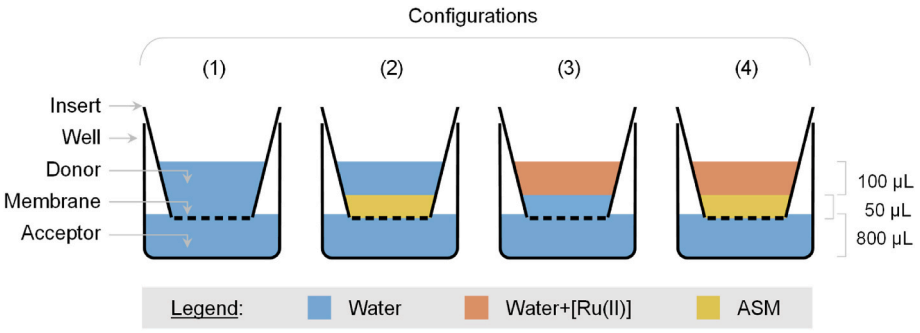

Fig. 3. Schematic representation of the diffusion set-up according to the different configurations evaluated. The thickness of the ASM layer was about 1 mm. The configuration depicted in (4) was used to monitor the diffusion of [Ru(II)] from the donor (upper) compartment to the acceptor (lower) compartment through an intermediate ASM layer. The other configurations (1–3) were used as controls to interpret the results obtained in (4).

tests were done using NaCl instead of ASM, as we previously showed that [Ru(II)]-based PDT effects could be obtained in that medium [31]. After illumination of mixtures of a given [Ru(II)] with bacteria in either of these two media, growth kinetics were carried out to determine the number of surviving cells [30]. In any case, no effect was observed when samples were kept in the dark (i.e. in the absence of light), thus reporting no detectable dark toxicity due to the compounds evaluated. (i) In NaCl, upon light treatment, **[Ru(II)] 1** reduced the bacterial load of *S. aureus* by about one log10 whereas it fully eradicated *P. aeruginosa* (five log10 reduction), in accordance with previous findings [31]. When using **[Ru(II)] 2**, no effect was found with *S. aureus* whereas one log10 reduction was measured with *P. aeruginosa*. (ii) In ASM, no aPDT effect was detected, regardless of the [Ru(II)] and the bacteria tested (Fig. 4). These results thus highlighted that both [Ru(II)] can photo-inactivate planktonic cells of *S. aureus* and *P. aeruginosa* in simple (saline) condition, but not in ASM.

3.1.2. Characterization of [Ru(II)] in ASM

[Ru(II)] were then evaluated with regards to (i) their potential interactions with ASM as well as (ii) their ability to generate $^1O_2$ in the latter. For these tests, [Ru(II)] were first incubated with ASM then a centrifugation was performed to pellet high molecular weight compounds and their aggregates potentially formed with [Ru(II)]. As control, same experiments were performed in water (instead of ASM).

As for interaction, [Ru(II)] was quantitated by measuring OD at 455 nm and processing a range of known [Ru(II)] quantities in parallel (Figs. S1A–B). In water, both [Ru(II)] did not precipitate and they were only detected in solution (no pellet being formed). The concentrations estimated in solutions were ~50 µM, corresponding to that used in the assay and confirming that compounds remained as a soluble fraction. In the presence of ASM, although [Ru(II)] were mostly found in the supernatant, they could also be detected in the pellets formed with ASM components (Fig. 5A). These results highlighted that both [Ru(II)] can interact to some extent with some of the latter. Complementary tests suggested that this interaction mostly involved the mucin that is contained in ASM (Figs. S3A–B).

As for $^1O_2$ detection, the SOSG fluorescence upon light treatment was normalized to that in corresponding control conditions (i.e. the fluorescence of that probe in water or in ASM – in the absence of any [Ru(II)] – was set to 1; Fig. S2). This allowed to determine relative SOSG fluorescence signals in a given condition, which above 1 (i.e. above the detection threshold) were considered reporting the production of $^1O_2$. In water, the relative fluorescence was significantly higher than 1 with both [Ru(II)]. However in ASM, no or only weak SOSG fluorescence could be measured, whether in the supernatant or in the pellet fraction (Fig. 5B). Complementary assays were done to determine the ability to detect $^1O_2$ when [Ru(II)] were mixed with individual ASM components. It appeared that this detection was lower in the presence of DNA and mucin than in the presence of any other component (Figs. S3C–D), which may be explained in different ways (see discussion).

3.2. Impact after diffusion across ASM

3.2.1. PDT efficiency

The ability of [Ru(II)] to mediate bacterial PDI was evaluated after diffusion through an ASM layer (using a Transwell assembly, as described in Materials and Methods, see Fig. 3). For this purpose, [Ru(II)] was first introduced in the donor compartment then let to passively diffuse though the insert membrane into the acceptor compartment. After 4 h at RT, an aliquot from the latter was collected and used to perform PDT assays, following the same protocol as that described before. As control, water instead of ASM was used in experiments conducted in parallel (Fig. 3 configuration (3)). In the latter condition, it was found that for both [Ru(II)], slight but statistically significant PDI

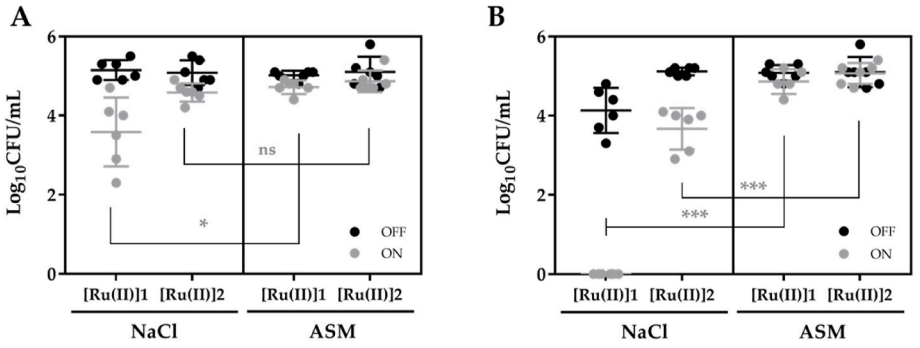

Fig. 4. [Ru(II)]-PDI of planktonic *S. aureus* (A) and *P. aeruginosa* (B) either in NaCl or in ASM. In every test, bacteria were treated with 25 µM of [Ru(II)] and either kept in the dark (OFF) or exposed to light (ON). The results correspond to (N = 2, n = 3) with statistical analysis done using the Student's t-test (***, p-value ≤0.001; **, p-value ≤0.01; *, p-value ≤0.05; ns, not significant).

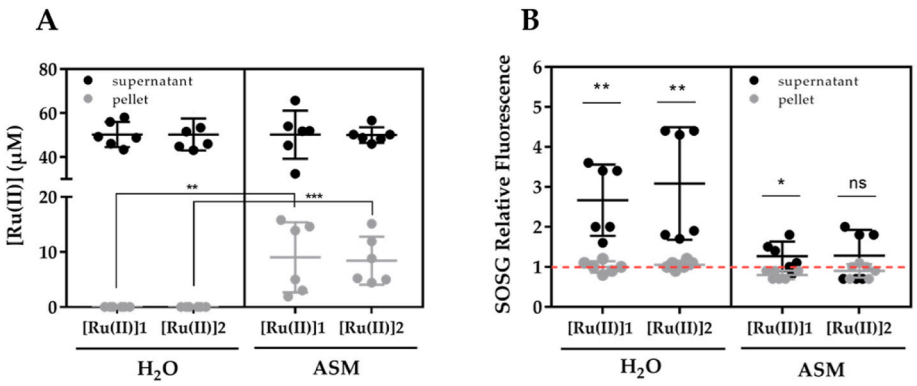

Fig. 5. Determination of [Ru(II)] concentration (A) and relative detection of singlet oxygen production (B) either in water or in ASM, and following centrifugation to separate the supernatant from the pellet. In every test, the concentration of [Ru(II)] before centrifugation was 50 μM. The red dashed line in (B) denotes the $^1O_2$ detection threshold (SOSG fluorescence in the absence of any [Ru(II)] set to 1). These results correspond to mean ± SD (N = 2, n = 3) with statistical analysis done using the Student's t-test (***, p-value ≤0.001; **, p-value ≤0.01; *, p-value ≤0.05; ns, not significant).

effects against *S. aureus* could be measured, meaning that these PS were still photoactivable and present at sufficient concentrations in the samples evaluated; against *P. aeruginosa*, such effect could be measured only with **[Ru(II)] 1** (Fig. 6). Following diffusion across the ASM layer (Fig. 3 configuration (4)), no bacterial PDI was measured in any condition examined, irrespective of the [Ru(II)] and the bacteria tested (Fig. 6).

3.2.2. Characterization of [Ru(II)] after diffusion

In every condition tested, both [Ru(II)] could be detected to some extent in the acceptor compartment, indicating their ability to diffuse through the insert membrane. In the absence of ASM, the concentration of either of the two [Ru(II)] in the donor compartment was ~4 fold higher than in the acceptor compartment. In the presence of ASM, both [Ru(II)] could also reach the acceptor compartment but with a strongly reduced efficiency; the concentrations of **[Ru(II)] 1** and **[Ru(II)] 2** in the acceptor compartment was indeed ~ 47 and ~18 times lower than that determined in the donor compartment. Thus, the presence of ASM significantly reduced the diffusion of [Ru(II)], the concentrations they reached in the acceptor compartment being 19% (**Ru(II)] 1**) and 37% (**[Ru(II)] 2**) that determined in the absence of that layer (Fig. 7A).

The results obtained with the SOSG probe suggested that, in the absence of ASM, the production of $^1O_2$ could be detected in both compartments; this production could be estimated to be on average 2–3 fold higher in the donor than in the acceptor compartment. This was in quite good accordance with the difference of concentrations of [Ru(II)] previously determined on both sides of the membrane (Fig. 7A). When ASM was added to the setup, the relative SOSG fluorescence signal was strongly reduced, suggesting that $^1O_2$ was not produced or at very low levels, not only in the acceptor but also in the donor compartment (Fig. 7B). These results were actually consistent with our previous findings showing that ASM impacted on SOSG fluorescence (Fig. 5B), which could be explained in different ways and inform about various situations (see Discussion).

3.3. Impact of biofilms

3.3.1. aPDT against bacteria in biofilms

[Ru(II)] were then evaluated considering their ability to photoinactivate *S. aureus* or *P. aeruginosa* growing in biofilms formed in ASM. Here for comparative purposes, the same tests were done using LB instead of ASM. Considering that [Ru(II)] hardly diffuse through bacterial biofilms [31], a "pre-delivery eradication assay" was conducted that consisted in premixing bacteria with [Ru(II)] before the addition of either LB or ASM and an overnight incubation under static conditions. By this way, [Ru(II)] were at least in part embedded in the biofilms subsequently formed, thus overcoming the limitation due to their poor diffusion in this layer. In every condition, crystal violet staining confirmed the ability of bacteria to form biofilms, irrespective of the presence of [Ru(II)] (data not shown). After biofilm formation, the upper phase containing planktonic cells was carefully discarded to isolate the biofilm attached phase at the bottom of each well. Following light treatment, biofilms were mechanically disrupted to expectedly obtain isolated (single) bacteria that could be counted via serial dilutions. From the results obtained, when considering first biofilms formed in LB, **[Ru(II)] 1** was found effective to reduce the bacterial load of *P. aeruginosa* and *S. aureus*, as reported earlier [31]; **[Ru(II)] 2** was found also efficient, but only against *S. aureus*. When considering biofilms formed in ASM, both [Ru(II)] were ineffective towards *S. aureus*; only **[Ru(II)] 1** showed some efficiency against *P. aeruginosa* (Fig. 8). These results thus further pointed out the negative impact of ASM on [Ru(II]-based aPDT when biofilm is formed in that medium, which may be explained in

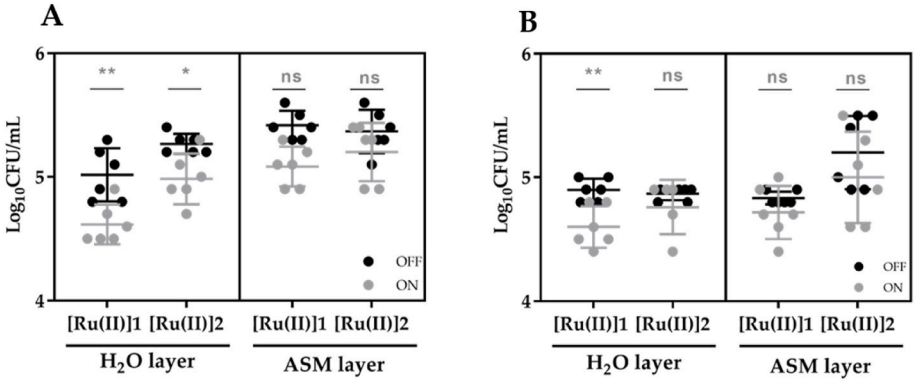

Fig. 6. [Ru(II)]-PDI of planktonic *S. aureus* (A) and *P. aeruginosa* (B) using samples collected from the acceptor compartment after diffusion through water or an ASM layer (as described in Fig. 3). In every test, the concentration of [Ru(II)] in the acceptor compartment before diffusion was 50 μM. These results correspond to mean ± SD (N = 2, n = 3) with statistical analysis done using the Student's t-test (***, p-value ≤0.001; **, p-value ≤0.01; *, p-value ≤0.05; ns, not significant).

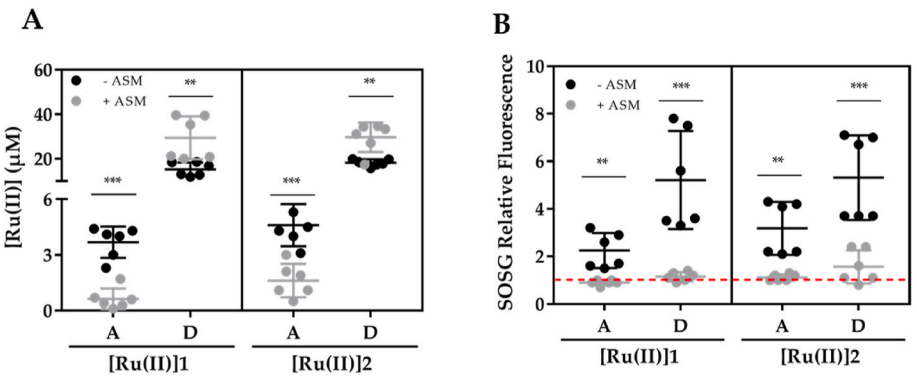

Fig. 7. Determination of [Ru(II)] concentration (A) and relative detection of singlet oxygen production (B) in samples collected from the donor – D – and acceptor – A – compartments after diffusion for 4 h. In every test, the concentration of [Ru(II)] in the acceptor compartment before diffusion was 50 µM. The red dashed line in (B) denotes the $^1O_2$ detection threshold (SOSG fluorescence in the absence of any [Ru(II)] set to 1). These results correspond to mean ± SD (N = 2, n = 3) with statistical analysis done using the Student's t-test (***, p-value ≤0.001; **, p-value ≤0.01; *, p-value ≤0.05; ns, not significant).

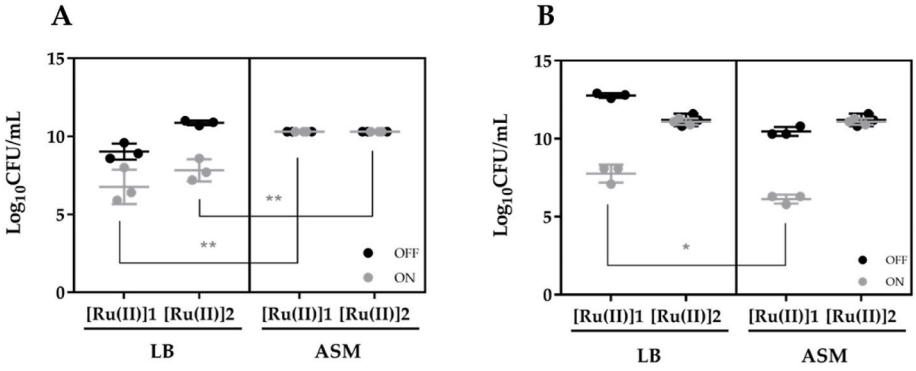

Fig. 8. [Ru(II)]-PDI of *S. aureus* (A) and *P. aeruginosa* (B) in biofilms formed in the presence of [Ru(II)]. In every test, the concentration of [Ru(II)] mixed with bacteria before setting up biofilms was 50 µM. These results correspond to (N = 1, n = 3) with statistical analysis done using the Student's t-test (***, p-value ≤0.001; **, p-value ≤0.01; *, p-value ≤0.05; ns, not significant).

different ways (see below and Discussion).

3.3.2. *Characterization of [Ru(II)] in biofilms*

The concentration of [Ru(II)] in biofilms was determined by using the same protocol as that used in ASM, except that fluorescence instead of absorption measurements were here done and the background signal due to biofilm alone was subtracted (see section 2.2.3 and Figs. S1C–D). In every condition, [Ru(II)] could be detected in biofilms, for quite low concentrations (in the µM range). When *S. aureus* biofilms were formed in LB or ASM, similar concentrations of both compounds could be found. With *P. aeruginosa*, concentrations were slightly higher when biofilms were formed in ASM than in LB (Fig. 9A).

The measurements done using the SOSG showed that, for both [Ru(II)], $^1O_2$ could be detected in *S. aureus* biofilms formed in LB. As for *P. aeruginosa* biofilms formed in LB, **[Ru(II)]1** but not **[Ru(II)]2** allowed to detect the production of $^1O_2$, although it was much weaker and not statistically different from the control condition. When assaying biofilms formed in ASM, no or very weak $^1O_2$ production could be measured in any case, irrespective of the [Ru(II)] and bacteria used (Fig. 9B).

All combined, the results obtained under the various experimental conditions examined shed more light on the [Ru(II)]-mediated bacterial PDI, pointing out limitations related to the available dose of these PS and their ability to produce $^1O_2$ (Table S1).

4. Discussion

The development of new antimicrobial treatments implies understanding the drug behavior in the target microenvironment, which is characterized by specific pathophysiological disturbances in infected

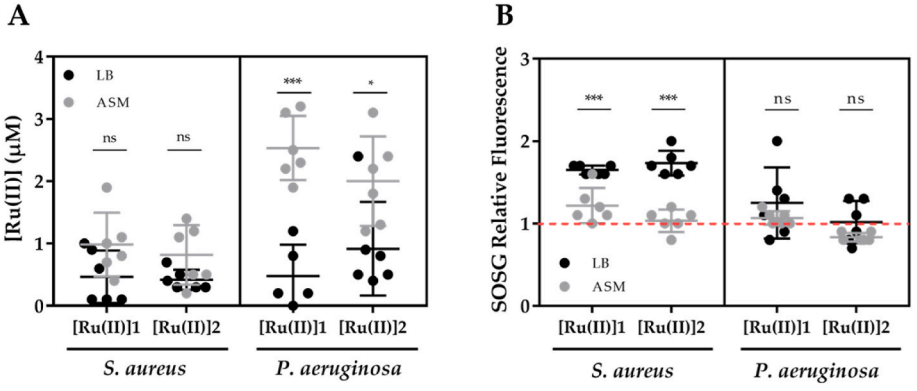

Fig. 9. Determination of [Ru(II)] concentration (A) and relative detection of singlet oxygen production (B) inside biofilms formed 24 h after incubation of bacteria premixed with a given [Ru(II)]. In every test, the concentration of [Ru(II)] mixed with bacteria before setting up biofilms was 50 µM. The red dashed line in (B) denotes the $^1O_2$ detection threshold (SOSG fluorescence in the absence of any [Ru(II)] set to 1). These results correspond to mean ± SD (N = 2, n = 3) with statistical analysis done using the Student's t-test (***, p-value ≤0.001; **, p-value ≤0.01; *, p-value ≤0.05; ns, not significant).

pulmonary airways [30,31,33]. The effectiveness of antimicrobials can indeed be modulated by extracellular materials present at the lining of the pulmonary epithelium, in particular biofilms and mucus in patients with CF [33]. Several studies have shown that, in general, the effect of antibiotics is greater in a simple, well-defined medium, such as LB or Muller Hinton Broth, than in a synthetic more complex medium such as ASM mimicking the mucus found in the CF lungs [34].

In the present study, ruthenium (II) complexes were evaluated to determine to which extent mucus and biofilms can impact on their antimicrobial photodynamic activity. Two compounds noted **[Ru(II)] 1** and **[Ru(II)] 2** were used, which only differed according to the nature of their bidental ligand i.e. 1,10-phenantroline and 2,2'-bipyridine, respectively (Fig. 2). They were selected considering their relatively low molecular weight and high water solubility compared to other derivatives previously evaluated [30,31]. These properties may allow a higher mobility when passing through ASM and biofilm layers [33]. In spite of apparently minor chemical variations, these compounds could yield different results under the various experimental settings considered. In water or in saline, both compounds were efficient to photo-inactivate *S. aureus* and *P. aeruginosa* growing as planktonic cells (Fig. 4). However, **[Ru(II)] 1** demonstrated some better antimicrobial activities in comparison to **[Ru(II)] 2**, which could be related to difference in terms of fluorescence and $^1O_2$ production (Fig. S3). In the presence of mucus and biofilms, other differences could be highlighted between **[Ru(II)] 1** and **[Ru(II)] 2**, but for both it was consistently found that bacterial PDI was strongly affected. This could result from various mechanisms, involving the components contained in these media impacting on the diffusion, interaction(s) and local available quantities of [Ru(II)] as well as the photo-activation of the latter, as detailed below.

The diffusion of [Ru(II)] in ASM depends on many parameters and can be impacted in different ways. In addition to DNA, the mucin contained in ASM could interact and aggregate with [Ru(II)], via electrostatic interactions involving the negative charges of these biopolymers and the positive charges of [Ru(II)]. We found that both [Ru(II)] could indeed interact with mucin, the latter showing a higher affinity for **[Ru(II)] 1** than **[Ru(II)] 2** (Figs. S3A–B). As a result of such interactions, diffusion of [Ru(II)] through the ASM layer can be strongly compromised. In the tests conducted with our experimental setup (Fig. 3), we estimated that 11 and 27% of the total amount of **[Ru(II)] 1** and **[Ru(II)] 2** introduced in the donor compartment were able to cross a 1 mm layer of ASM and reach the acceptor compartment (in the absence of ASM, diffusion yields were 59 and 74%, respectively) (Fig. 7A). **[Ru(II)] 2** being less prone to interact with ASM than **[Ru(II)] 1** (Figs. S3A–B), it may be slightly more efficient to diffuse through this layer (Fig. 7A). As a comparison, Donnelly et al. reported that ~50% of the total amount of toluidine blue O (TBO) or meso-tetra (N-methyl-4-pyridyl)porphine tetratosylate (TMP) introduced in the donor compartment of a Franz cell were able to diffuse across 3 mm of artificial CF mucus after 6 h [35]. Experimental settings must be carefully considered to interpret the results obtained. In our tests, the diffusion of [Ru(II)] from the donor to the receptor compartments resulted from sedimentation and difference of concentrations, but also the physico-chemical properties of these compounds. The hydrophobic/hydrophilic balance plays a key role (our tests having been done in aqueous media and the membrane of the insert being made of polyester (PET), a hydrophobic material). Less hydrophilic [Ru(II)] than those used herein would probably yield lower diffusions, as suggest tests done with another derivative (featuring a LogP = 0.14, to be compared with LogP **[Ru(II)] 1** = −2.02) that was unable to diffuse in this model (possibly due to aggregation and deposition on – and collapse of – the insert membrane; data not shown). Furthermore, it is noteworthy that ASM could slightly diffuse from the donor to the acceptor compartment after 4 h; ASM could thus both interact and trap [Ru(II)] but also participate in its diffusion, acting like a drug carrier under the set-up conditions used.

The diffusion of [Ru(II)] in biofilms constitutes another bottleneck. In a previous study, we showed that [Ru(II)] were poorly efficient to exert PDI on bacteria in biofilms, which was ascribed to a poor diffusion of these PS in the latter [31]. Interestingly, if bacteria were first mixed with [Ru(II)] in saline (to optimize their interaction) then cultivated in LB to form a biofilm, it was possible to measure some antibacterial effects upon light exposure (Fig. 8). This finding points that, under such experimental condition, [Ru(II)] can stay close to – and/or entrapped in – bacteria while retaining properties allowing them to be photo-activated. It also suggests that even if bacteria are embedded in EPS in biofilms, they could be the target of ROS produced by [Ru(II)] provided that these compounds are able to "safely" diffuse and get close to them. Interestingly, the use of ASM (instead of LB) to grow biofilms using bacteria premixed in saline with [Ru(II)] did not yield such results i.e. no bacterial PDI could be measured (Fig. 8). ASM could act as a stronger anion than bacteria for electrostatic interaction with [Ru(II)], an hypothesis that should be tested in another study.

The photo-stability of [Ru(II)] may also be compromised in the presence of mucus and biofilms. In addition to inducing their aggregation, the many components contained in these complex media could alter [Ru(II)] in different ways. Interaction tests indicated that, depending on the individual ASM components but also the [Ru(II)] examined, the $^1O_2$ production could strongly vary; However, it was noticeable that for both compounds, this production was the most reduced in the presence of mucin (Figs. S3C–D). In mixture with all ASM components, $^1O_2$ was hardly detectable, with much lower signals than in water (Fig. S2). The detection of this radical species is technically complex. In the present study, the SOSG was used as a chemical probe to report – via fluorescence – the generation of $^1O_2$. It is important to notice that our results did not allow to distinguish between the actual ability of [Ru(II)] to produce $^1O_2$ upon illumination from our ability to detect its production in the various experimental conditions examined (in particular in the presence of ASM). Furthermore, fluorescence interferences (e.g. quenching effect) and/or $^1O_2$ consumption before reaction with SOSG could also occur. Noticeably, no fluorescence increase was observed in any experimental condition examined. Alternative protocols may be used in future studies, making use of (i) other probes (e.g. DPBF or ABDA [36]) and/or (ii) other detection methods (e.g. based on the measurement of $^1O_2$ phosphorescence [30,37]). Besides $^1O_2$, the production of other ROS may also be impacted by mucus and biofilm components, which could be investigated using other protocols and detection probes such as 2′,7′-dichlorofluorescin diacetate (DCFH-DA) [31].

The photo-activation of [Ru(II)] relies on their exposure to light, which may also be affected in a complex medium such as ASM (or biofilms) where light transmittance is reduced (notably due to scattering and absorbing effects) [31]. Compared to other studies, light treatment was herein performed using relatively low power and short exposure durations; these could be increased to obtain stronger PDI effects, while still avoiding any photo-bleaching of [Ru(II)] and any side-effects for the host.

Combining our results with other findings from a recent report studying the impact of lung surfactant [33], we can hypothesize that the decreased bacterial PDI in ASM and in biofilms are not primarily due to $^1O_2$ quenching but rather undesired interactions subsequently impacting on the uptake of [Ru(II)] by target bacteria. This work further corroborates that the multiple components in the lung micro-environment must be carefully taken into account to design efficient aPDT strategies. From another point of view, inhibitor components in mucus and/or biofilms may be reconsidered as "helpers" for improving the trafficking and delivery of [Ru(II)], following a rationale similar to that used in other studies [38–41].

5. Conclusion

This study aimed to point out the possible impacts of mucus and

biofilm components on [Ru(II)]-based aPDT. We used a series of methods and protocols that, following additional improvements, may be useful for future similar studies. In spite of some technical limitations, our results clearly highlight the critical impacting role of components in mucus and biofilms, which may prevent the activity of [Ru(II)] before they could act on target bacteria, by sequestering these PS and/or compromising their photochemical properties. From these points of views, there is ample room for improvements, from the chemical engineering to the formulation of [Ru(II)] [33,42]. This may allow to limit undesired interactions with environmental components, but also to improve absorption at higher wavelengths more efficient to cross complex media and more compatible for noninvasive (extracorporeal) illumination [19,43].

Fundings

Financial supports were obtained from ANR (TARGET-THERAPY project, grant number: ANR-20-AMRB-0009, RPV21103NNA), "Association de Transfusion Sanguine et de Biogénétique Gaétan Saleün" (France), and the "Conseil Régional de Bretagne" (France). Raphaëlle Youf was a recipient of a PhD fellowship from the French "Ministère de l'Enseignement supérieur, de la Recherche et de l'Innovation" (Paris, France).

Role of the funding source

The funding sources had no role in the design of this study and during its execution, analyses, interpretation of the data, or decision to submit results.

CRediT authorship contribution statement

Raphaëlle Youf: Conceptualization, Methodology, Software, Data curation, Writing – original draft, Visualization, Investigation, Validation, Writing – review & editing. **Rosy Ghanem:** Conceptualization, Methodology, Software, Visualization, Validation, Writing – review & editing. **Adeel Nasir:** Visualization, Validation, Writing – review & editing. **Gilles Lemercier:** Visualization, Validation, Writing – review & editing. **Tristan Montier:** Visualization, Validation, Writing – review & editing. **Tony Le Gall:** Conceptualization, Methodology, Software, Data curation, Writing – original draft, Visualization, Supervision, Investigation, Validation.

Declaration of competing interest

The authors declare that they have no conflict of interest.

Data availability

Data will be made available on request.

Acknowledgements

We are grateful to Lhousseine Touqui and Frédéric Tewes for scientific support and expertise. We also acknowledge Alizé Hascoët for technical assistance.

Appendix A. Supplementary data

Supplementary data to this article can be found online at https://doi.org/10.1016/j.bioflm.2023.100113.

References

[1] GBD 2016 lower respiratory infections collaborators estimates of the global, regional, and national morbidity, mortality, and aetiologies of lower respiratory infections in 195 countries, 1990-2016: a systematic analysis for the global burden of disease study 2016. Lancet Infect Dis 2018;18:1191–210. https://doi.org/10.1016/S1473-3099(18)30310-4.

[2] Di Martino P. Extracellular polymeric substances, a key element in understanding biofilm phenotype. AIMS Microbiol 2018;4:274–88. https://doi.org/10.3934/microbiol.2018.2.274.

[3] Flemming H-C, Neu TR, Wozniak DJ. The EPS matrix: the "house of biofilm cells. J Bacteriol 2007;189:7945–7. https://doi.org/10.1128/JB.00858-07.

[4] Morrison CB, Markovetz MR, Ehre C Mucus. Mucins and cystic fibrosis. Pediatr Pulmonol 2019;54:S84–96. https://doi.org/10.1002/ppul.24530.

[5] Csanády L, Vergani P, Gadsby DC. Structure, gating, and regulation of the CFTR anion channel. Physiol Rev 2019;99:707–38. https://doi.org/10.1152/physrev.00007.2018.

[6] Castellani C, Assael BM. Cystic fibrosis: a clinical view. Cell Mol Life Sci 2017;74:129–40. https://doi.org/10.1007/s00018-016-2393-9.

[7] Ratjen F, Döring G. Cystic fibrosis. Lancet 2003;361:681–9. https://doi.org/10.1016/S0140-6736(03)12567-6.

[8] Bossche SV den, Broe ED, Coenye T, Braeckel EV, Crabbé A. The cystic fibrosis lung microenvironment alters antibiotic activity: causes and effects. Eur Respir Rev 2021;30. https://doi.org/10.1183/16000617.0055-2021.

[9] Lin, Q. Cystic fibrosis acidic microenvironment determines antibiotic susceptibility and biofilm formation of Pseudomonas aeruginosa. 29.

[10] Jurado-Martín I, Sainz-Mejías M, McClean S. Pseudomonas aeruginosa: an audacious pathogen with an adaptable arsenal of virulence factors. Int J Mol Sci 2021;22:3128. https://doi.org/10.3390/ijms22063128.

[11] Lund-Palau H, Turnbull AR, Bush A, Bardin E, Cameron L, Soren O, Wierre-Gore N, Alton EWFW, Bundy JG, Connett G, et al. *Pseudomonas aeruginosa* infection in cystic fibrosis: pathophysiological mechanisms and therapeutic approaches. Expet Rev Respir Med 2016;10:685–97. https://doi.org/10.1080/17476348.2016.1177460.

[12] Kamble E, Pardesi K. Antibiotic tolerance in biofilm and stationary-phase planktonic cells of Staphylococcus aureus. Microb Drug Resist 2021;27:3–12. https://doi.org/10.1089/mdr.2019.0425.

[13] Mah T-F, Pitts B, Pellock B, Walker GC, Stewart PS, O'Toole GA. A genetic basis for Pseudomonas aeruginosa biofilm antibiotic resistance. Nature 2003;426:306–10. https://doi.org/10.1038/nature02122.

[14] Müller L, Murgia X, Siebenbürger L, Börger C, Schwarzkopf K, Sewald K, Häussler S, Braun A, Lehr C-M, Hittinger M, et al. Human airway mucus alters susceptibility of Pseudomonas aeruginosa biofilms to tobramycin, but not colistin. J Antimicrob Chemother 2018;73:2762–9. https://doi.org/10.1093/jac/dky241.

[15] Dinwiddie R. Anti-inflammatory therapy in cystic fibrosis. J Cyst Fibros 2005;4:45–8. https://doi.org/10.1016/j.jcf.2005.05.010.

[16] Hassett DJ, Sutton MD, Schurr MJ, Herr AB, Caldwell CC, Matu JO. Pseudomonas aeruginosa hypoxic or anaerobic biofilm infections within cystic fibrosis airways. Trends Microbiol 2009;17:130–8. https://doi.org/10.1016/j.tim.2008.12.003.

[17] Suk JS, Kim AJ, Trehan K, Schneider CS, Cebotaru L, Woodward OM, Boylan NJ, Boyle MP, Lai SK, Guggino WB, et al. Lung gene therapy with highly compacted DNA nanoparticles that overcome the mucus barrier. J Contr Release 2014;178:8–17. https://doi.org/10.1016/j.jconrel.2014.01.007.

[18] Bradley BT, Bryan A. Emerging respiratory infections: the infectious disease pathology of SARS, MERS, pandemic influenza, and Legionella. Semin Diagn Pathol 2019;36:152–9. https://doi.org/10.1053/j.semdp.2019.04.006.

[19] Díaz Tovar JS, Kassab G, Buzzá HH, Bagnato VS, Kurachi C. Photodynamic inactivation of Streptococcus pneumoniae with external illumination at 808 Nm through the ex vivo porcine thoracic cage. J Biophot 2022;15:e202100189. https://doi.org/10.1002/jbio.202100189.

[20] Almeida A, Faustino MAF, Neves MGPMS. Antimicrobial photodynamic therapy in the control of COVID-19. Antibiotics (Berlin) 2020;9:E320. https://doi.org/10.3390/antibiotics9060320.

[21] Youf R, Müller M, Balasini A, Thétiot F, Müller M, Hascoët A, Jonas U, Schönherr H, Lemercier G, Montier T, et al. Antimicrobial photodynamic therapy: latest developments with a focus on combinatory strategies. Pharmaceutics 2021;13:1995. https://doi.org/10.3390/pharmaceutics13121995.

[22] Alves, E.; Faustino, M.A.; Neves, M.G.; Cunha, A.; Tome, J.; Almeida, A. An insight on bacterial cellular targets of photodynamic inactivation. Future Med Chem 6, 141–164.

[23] Abrahamse H, Hamblin MR. New photosensitizers for photodynamic therapy. Biochem J 2016;473:347–64. https://doi.org/10.1042/BJ20150942.

[24] Polat E, Kang K. Natural photosensitizers in antimicrobial photodynamic therapy. Biomedicines 2021;9:584. https://doi.org/10.3390/biomedicines9060584.

[25] Munteanu A-C, Uivarosi V. Ruthenium complexes in the fight against pathogenic microorganisms. An extensive review. Pharmaceutics 2021;13:874. https://doi.org/10.3390/pharmaceutics13060874.

[26] Knežević NŽ, Stojanovic V, Chaix A, Bouffard E, Cheikh KE, Morère A, Maynadier M, Lemercier G, Garcia M, Gary-Bobo M, et al. Ruthenium(II) complex-photosensitized multifunctionalized porous silicon nanoparticles for two-photon near-infrared light responsive imaging and photodynamic cancer therapy. J Mater Chem B 2016;4:1337–42. https://doi.org/10.1039/C5TB02726H.

[27] Li F, Collins JG, Keene FR. Ruthenium complexes as antimicrobial agents. Chem Soc Rev 2015;44:2529–42. https://doi.org/10.1039/c4cs00343h.

[28] Josefsen LB, Boyle RW. Photodynamic therapy and the development of metal-based photosensitisers. Met Base Drugs 2008;2008:1–23. https://doi.org/10.1155/2008/276109.

[29] Frei A. Metal complexes, an untapped source of antibiotic potential? Antibiotics 2020;9:90. https://doi.org/10.3390/antibiotics9020090.

[30] Le Gall T, Lemercier G, Chevreux S, Tücking K-S, Ravel J, Thétiot F, Jonas U, Schönherr H, Montier T. Ruthenium(II) polypyridyl complexes as photosensitizers for antibacterial photodynamic therapy: a structure-activity study on clinical bacterial strains. ChemMedChem 2018;13:2229–39. https://doi.org/10.1002/cmdc.201800392.

[31] Youf R, Nasir A, Müller M, Thétiot F, Haute T, Ghanem R, Jonas U, Schönherr H, Lemercier G, Montier T, et al. Ruthenium(II) polypyridyl complexes for antimicrobial photodynamic therapy: prospects for application in cystic fibrosis lung airways. Pharmaceutics 2022;14:1664. https://doi.org/10.3390/pharmaceutics14081664.

[32] Sriramulu DD, Lünsdorf H, Lam JS, Römling U. Microcolony Formation: a novel biofilm model of Pseudomonas aeruginosa for the cystic fibrosis lung. J Med Microbiol 2005;54:667–76. https://doi.org/10.1099/jmm.0.45969-0. 2005.

[33] Kassab G, Diaz Tovar JS, Souza LMP, Costa RKM, Silva RS, Pimentel AS, Kurachi C, Bagnato VS. Lung surfactant negatively affects the photodynamic inactivation of bacteria-in vitro and molecular dynamic simulation analyses. Proc Natl Acad Sci U S A 2022;119:e2123564119. https://doi.org/10.1073/pnas.2123564119.

[34] Diaz Iglesias Y, Van Bambeke F. Activity of antibiotics against Pseudomonas aeruginosa in an in vitro model of biofilms in the context of cystic fibrosis: influence of the culture medium. Antimicrob Agents Chemother 2020;64:e02204–19. https://doi.org/10.1128/AAC.02204-19.

[35] Donnelly RF, McCarron PA, Cassidy CM, Elborn JS, Tunney MM. Delivery of photosensitisers and light through mucus: investigations into the potential use of photodynamic therapy for treatment of Pseudomonas aeruginosa cystic fibrosis pulmonary infection. J Contr Release 2007;117:217–26. https://doi.org/10.1016/j.jconrel.2006.11.010.

[36] Entradas T, Waldron S, Volk M. The detection sensitivity of commonly used singlet oxygen probes in aqueous environments. J Photochem Photobiol B Biol 2020;204:111787. https://doi.org/10.1016/j.jphotobiol.2020.111787.

[37] Ossola R, Jönsson OM, Moor K, McNeill K. Singlet oxygen quantum yields in environmental waters. Chem Rev 2021;121:4100–46. https://doi.org/10.1021/acs.chemrev.0c00781.

[38] Egesten A, Herwald H. The extracellular matrix: reloaded revolutions. J Innate Immun 2019;11:301–2. https://doi.org/10.1159/000500357.

[39] Roy R, Tiwari M, Donelli G, Tiwari V. Strategies for combating bacterial biofilms: a focus on anti-biofilm agents and their mechanisms of action. Virulence 2018;9:522–54. https://doi.org/10.1080/21505594.2017.1313372.

[40] Mitri C, Xu Z, Bardin P, Corvol H, Touqui L, Tabary O. Novel anti-inflammatory approaches for cystic fibrosis lung disease: identification of molecular targets and design of innovative therapies. Front Pharmacol 2020;11:1096. https://doi.org/10.3389/fphar.2020.01096.

[41] Banaschewski BJH, Veldhuizen EJA, Keating E, Haagsman HP, Zuo YY, Yamashita CM, Veldhuizen RAW. Antimicrobial and biophysical properties of surfactant supplemented with an antimicrobial peptide for treatment of bacterial pneumonia. Antimicrob Agents Chemother 2015;59:3075–83. https://doi.org/10.1128/AAC.04937-14.

[42] Anderski J, Mahlert L, Mulac D, Langer K. Mucus-penetrating nanoparticles: promising drug delivery systems for the photodynamic therapy of intestinal cancer. Eur J Pharm Biopharm 2018;129:1–9. https://doi.org/10.1016/j.ejpb.2018.05.018.

[43] Karges J, Kuang S, Maschietto F, Blacque O, Ciofini I, Chao H, Gasser G. Rationally designed ruthenium complexes for 1- and 2-photon photodynamic therapy. Nat Commun 2020;11:3262. https://doi.org/10.1038/s41467-020-16993-0.